https://doi.org/10.1016/j.cej.2019.123677

Interface engineering with a novel n-type small organic molecule for efficient inverted perovskite solar cells

Helin Wang[a,b,c,†], Fu Yang[a,d,e,†,*], Ning Li[d,f], Jun Song[a,*], Junle Qu[a], Shuzi Hayase[g], Wai-Yeung Wong[b,c,*]

[a] Key Laboratory of Optoelectronic Devices and Systems of Ministry of Education and Guangdong Province, College of Physics and Optoelectronic Engineering, Shenzhen University, Shenzhen 518060, Guangdong, P. R. China.

[b] Department of Applied Biology and Chemical Technology, The Hong Kong Polytechnic University, Hung Hom, Kowloon, Hong Kong, P. R. China.

[c] The Hong Kong Polytechnic University Shenzhen Research Institute, Shenzhen 518057, P. R. China.

[d] Institute of Materials for Electronics and Energy Technology (i-MEET), Friedrich-Alexander-Universität Erlangen-Nürnberg, Martensstrasse 7, 91058 Erlangen, Germany.

[e] Bavarian Center for Applied Energy Research (ZAE Bayern), Energy Campus Nürnberg, Fürther Straße 250, 90429 Nürnberg, Germany.

[f] National Engineering Research Center for Advanced Polymer Processing Technology, Zhengzhou University, 450002 Zhengzhou, China.

[g] Graduate School of Life Science and Systems Engineering Institution, Kyushu Institute of Technology, 2-4 Hibikino Wakamatsu-ku, Kitakyushu 808-0196, Japan.

[†] These two authors contributed this work equally.

[*] Corresponding authors.

E-mail: fu.yang@fau.de; songjun@szu.edu.cn; wai-yeung.wong@polyu.edu.hk.

Keywords: interface engineering; recombination loss; electron transport material; perovskite solar cell.

Abstract: Fullerene derivatives are promising electron transporting materials for low-temperature processed inverted perovskite solar cells (PSCs). However, fullerene derivatives

have some disadvantages, e.g. [6,6]-phenyl C_{61} butyric acid methyl ester (PCBM) has unmanageable morphology, low electron mobility and easily generated non-radiative recombination, which restrict the performance of PSCs. Herein, a novel n-type small organic molecule, homologous perylene diimide tetramer (HPDT), is designed and synthesized in this work to engineer the interface properties by enhancing interface contact, decreasing energetic barrier and recombination losses. HPDT shows suitable energy levels and high electron mobility and thus will increase the electron mobility when interface engineering in the inverted PSCs. Moreover, coating HPDT on top of perovskite prior to the deposition of PCBM is helpful to achieve a homogeneous pinhole-free PCBM layer, leading to enhanced power conversion efficiency from 17.38% up to 19.75% for inverted $MAPbI_3$ PSCs along with a negligible hysteresis. Significantly, our results undoubtedly enable new guidelines in exploring n-type organic small molecules for high-performance PSCs.

1. Introduction

Organometallic halide perovskite solar cells (PSCs) have gained intense attention owing to their rapid growing performance and favorable characteristics as optoelectronic materials [1-3]. Despite the fact that the power conversion efficiency (*PCE*) of PSCs has increased from 3.8% [4] to 25.2% [5] within the last decade, great effort is still required to promote PSCs from laboratory demonstration to industrial applications [6]. For instance, low-temperature, low-cost, high-throughput and scalable manufacturing processes which are greatly needed for commercialization of PSCs, are still far behind [7]. Moreover, some state-of-the-art electron transport materials (ETM) such as titanium dioxide (TiO_2) [8-11], tin dioxide (SnO_2) [12-19], zinc oxide (ZnO) [20-23], metal sulfide (CdS) [24], metal selenide (CdSe) [25], $BaSnO_3$ [26], and Nb_2O_5 [27] have been investigated by employing low-temperature processing and surface modification technologies. They have the advantages of high conductivity and excellent electron mobilities, thus promoting the development of the field of perovskite solar cells.

However, there are still some problems such as complex processing methods and poor chemical stability for inorganic ETM [28]. In addition, the performance of PSCs still suffer from surface trap states present at the inorganic ETM/perovskite interface which are responsible for charge recombination. Therefore, we have a strong desire to develop novel organic semiconductors for improving device performance and stability. Using n-type organic materials as electron transport layers (ETLs) in the inverted PSCs can overcome the above issues [29-31].

[6,6]-Phenyl C_{61} butyric acid methyl ester (PCBM) is the commonly utilized fullerene derivative in the inverted PSCs [32-36]. However, the use of PCBM as ETL would lead to additional recombination losses at the interface, limiting the performance potential of inverted PSCs. For instance, the fragmented coverage of PCBM on the perovskite results in severe non-radiative recombination owing to direct contact between the perovskite layer and the metal electrode [37]. This problem can be partially relieved by introducing another layer like lithium fluoride (LiF), 2,9-dimethyl-4,7-diphenyl-10-phenanthroline (BCP), and 4,7-diphenyl-1,10-phenanthroline (Bphen) to cap the PCBM surface [38-44]. Moreover, the unregulated energy level and low electron mobility of PCBM can also limit the performance of inverted PSCs, which could be addressed by replacing PCBM with non-fullerene materials with tunable energy level and electron mobility [45-48]. However, the small relative dielectric constant of PCBM creates a large electron capture region, which results in severe recombination at the interface between perovskite and PCBM layer [45].

In this work, we designed and synthesized a novel n-type organic molecule, homologous perylene diimide tetramer (HPDT), which can significantly modify the electronic properties at the perovskite/PCBM interface, leading to enhanced electron extraction and reduced recombination losses. The LUMO level of HPDT was estimated to be -4.04 eV which is well aligned to the conduction band of $MAPbI_3$ perovskite (-4.00 eV), compared to that of PCBM (-3.90 eV). As the nitrogen and sulfur atoms of HPDT could have strong intermolecular

interaction with Pb atoms of the perovskite, HPDT can effectively passivate to perovskite surface and would not be removed by the solvent during solution processing upper layers, which have proved by the X-ray photoelectron and photoluminescence results. Moreover, HPDT shows better electron mobility and the fragmented coverage of PCBM is avoided after interface engineering with HPDT which are proved by space charge limited current method and scanning electron microscopy results. As a result, the *PCE* of PSCs was greatly improved from 17.38% to 19.75% along with negligible hysteresis.

2. Results and Discussion

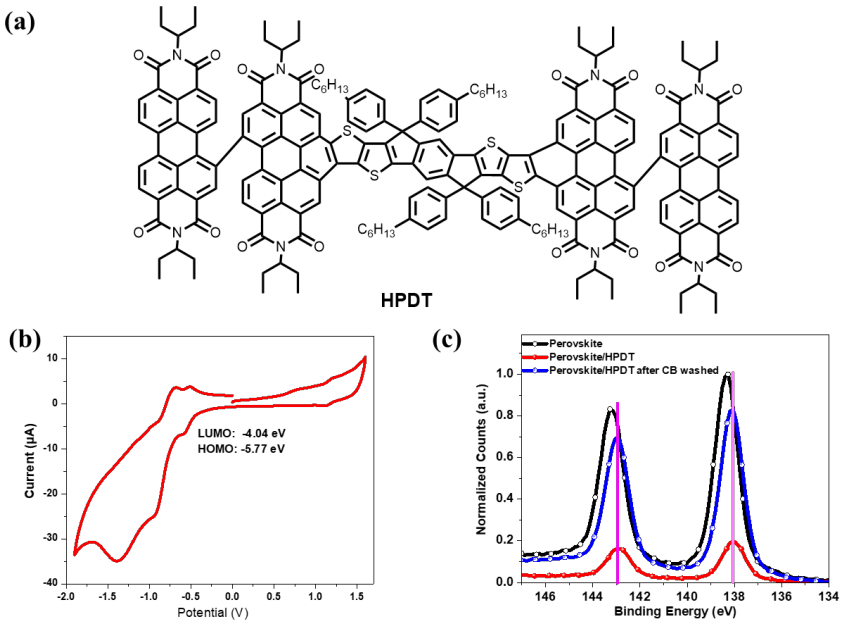

Figure 1. (a) Chemical structure and cyclic voltammetry (b) of HPDT; (c) XPS core level spectra of Pb 4f for $MAPbI_3$ perovskite film and perovskite film coated with a thin HPDT layer.

Figure 1a shows the chemical structure of the n-type small molecule, HPDT, a perylene diimide derivative combined with linear and ladder conjugated framework which highlights better electron transport than the other perylene diimide derivatives [49,50]. The synthetic route is detailed in the supporting information. The optical band gap (E_g) of HPDT was

calculated to be 1.73 eV using the onset of the absorption spectra (Figure S4). As shown in Figure 1b, the LUMO level of HPDT is -4.04 eV, which is well aligned to the conduction band of $MAPbI_3$ perovskite (-4.00 eV). The ground-state geometries were optimized by DFT calculations as shown in Figure S7. Figure 1c shows the X-ray photoelectron spectroscopy (XPS) spectra of perovskite films with and without HPDT. The peaks of Pb 4f slightly moved to the lower binding energy for the perovskite sample with a thin HPDT layer. The peaks are hardly influenced/removed by overcoating chlorobenzene (CB) indicating the strong intermolecular interaction between nitrogen and sulfur atoms of HPDT and Pb atoms of the perovskite [51,52]. From the above results, it is supposed that HPDT has the potential to work as the interlayer between perovskite and PCBM layer.

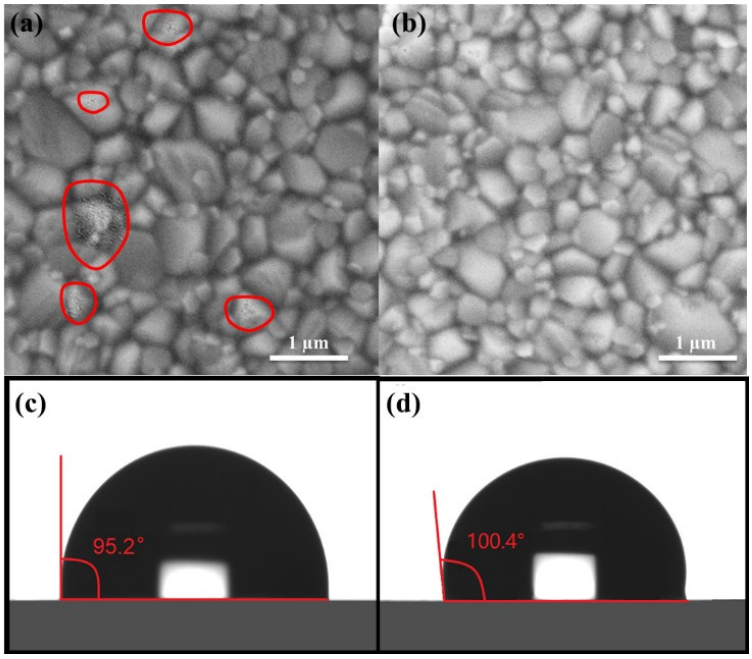

Figure 2. SEM images of the perovskite/PCBM (a) and perovskite/HPDT/PCBM (b) on ITO glass substrates; water contact angles of ITO/perovskite/PCBM (c) and ITO/perovskite/ HPDT (d) films.

Figures 2a and 2b show the top view of scanning electron microscopy (SEM) images of perovskite/PCBM and perovskite/HPDT/PCBM film. It is clear from Figure 2a that PCBM

suffers from fragmented coverage on the perovskite film. However, when a thin HPDT layer was inserted between the perovskite and PCBM layer, the PCBM layer shows a full coverage and pinhole-free film. In order to explain this phenomenon, the atomic force microscopy (AFM) was conducted (Figure S10). The root mean square (RMS) roughness of perovskite/HPDT film is 11.7 nm which is smoother than that of perovskite (18.4 nm). This could be one reason why interface engineering with HPDT could give the uniform and high-quality PCBM film, suggesting that interface engineering with HPDT can be beneficial for reducing the non-radiative recombination. Next, the water contact angle of perovskite/HPDT is higher than that of perovskite/PCBM as shown in Figure 2c and 2d, suggesting that interface engineering with HPDT can increase the stability of PSCs. This phenomenon is probably attributed to the nitrogen and sulfur atoms of HPDT, which could form hydrogen bonds to prevent water from entering into the perovskite layer [52].

Steady-state PL spectra were conducted, as shown in Figure 3a, to further study the effect of HPDT interface engineering. The perovskite/HPDT film shows a strong PL quenching compared to the pristine perovskite film, which indicates that efficient electron transfer occurred between the perovskite and HPDT layer. Furthermore, we compared the electron transport property of HPDT with PCBM by space charge limited current (SCLC) and organic field-effect transistors (OFET) methods. These results are shown in Figures S6 and S8. The electron mobility of two compounds was estimated to be 1.76×10^{-3} cm^2 V^{-1} s^{-1} for HPDT and 1.19×10^{-3} cm^2 V^{-1} s^{-1} for PCBM by the SCLC method. According to the OFET method, both two compounds showed n-channel transporting characteristics with the electron mobility of PCBM (1.51×10^{-2} cm^2 V^{-1} s^{-1}) and HPDT (1.26×10^{-2} cm^2 V^{-1} s^{-1}). The difference in their electron mobility obtained by OFET and SCLC is due to the different aggregation in the solid films. As far as we know, PCBM is more inclined to edge-on aggregation, and HPDT is more inclined to face-on aggregation. These results indicate that the electron transport property of HPDT is comparable to PCBM. Due to the existence of a larger conjugated framework,

HPDT has higher electron mobility than the perylene diimide dimer, trimer or tetramer reported by our group [53,54]. The above results suggest that HPDT could be an efficient electron transporting material. As shown in Figure S5, inverted PSCs incorporating HPDT only as the ETL could achieve an optimized *PCE* of 15.84%.

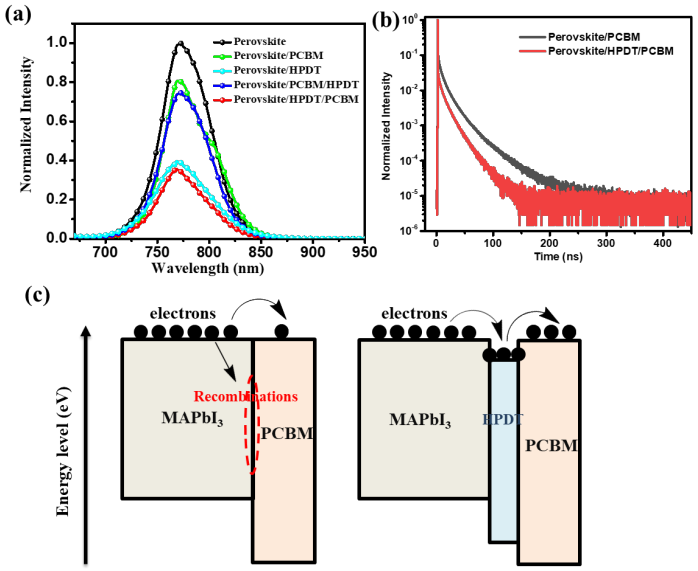

Figure 3. (a) Steady-state PL spectra for perovskite films covered by PCBM, HPDT, PCBM/HPDT or HPDT/PCBM layer; (b) TRPL spectra for perovskite films covered by PCBM or HPDT/PCBM layer; (c) working mechanism of HPDT interface engineering method.

In addition, perovskite/HPDT/PCBM film shows a stronger quenching effect than that of perovskite/PCBM, which proves that HPDT interface engineering could extract electron from perovskite film more efficiently. Furthermore, time-resolved photoluminescence (TRPL) spectra of perovskite/PCBM and perovskite/HPDT/PCBM were measured (Figure 3b). The TRPL decay curves were fitted with a bi-exponential decay function. Obviously, the perovskite/HPDT/PCBM film exhibits a decreased decay lifetime with t_1 (1.7 ns) and t_2 (6.6 ns) compared to perovskite/PCBM (t_1 and t_2 of 5.2 ns and 13.6 ns, respectively), which could be attributed to the increased electron extraction and digressive radiative recombination.

Figure 3c shows the working mechanism of this interface engineering method. HPDT could prevent the hole from moving to PCBM and improve the selectivity for the charge carrier transport which can result in less recombination and an increase in the charge collection efficiency.

To further explore the effect of HPDT interface engineering on the device performance, we fabricated the inverted planar PSCs with a structure of ITO/PTAA/PMMA/$MAPbI_3$/HPDT/ PCBM/Bphen/Al, as shown in Figure 4a. Figure 4b shows the *J-V* curves of PSCs with different thickness of HPDT layer. The detail parameters of the device performance are shown in Table 1. The inverted PSCs without HPDT exhibited low performance with a *PCE* of 17.15% due to the high recombination losses at the perovskite/PCBM interface. The performance of PSCs was improved to 19.16% and 19.75% by introducing 8 nm and 15 nm HPDT, respectively. The electron-only devices were carried out to evaluate the trap density and electron mobility of two perovskite films with or without HPDT layer (Figure S12). The perovskite/HPDT/PCBM film shows reduced trap density and improved electron mobility compared with the perovskite/PCBM film. These results could be attributed to the decreased charge recombination and improved interface contact while inserting a thin HPDT layer between the perovskite and PCBM layer.

Table 1. Device performance of perovskite solar cells with different thickness of HPDT.

Thickness [a] (nm)	J_{sc} [mA cm^{-2}]	V_{oc} [V]	*FF* [%]	*PCE* [%]
0	22.67	1.084	70.7	17.38
8	23.44	1.098	74.5	19.16
15	23.97	1.110	74.2	19.75
22	23.65	1.108	72.7	19.06

[a] The film thickness was measured by using a step meter.

Figure 4c shows the *J-V* curves of PSCs with or without HPDT in the forward and reverse scan. The origin of hysteresis in PSCs is usually due to the ionic motions within perovskite,

perovskite crystal defects, and band bending between the different interfaces. There is only negligible hysteresis in the PSCs with 15 nm HPDT owing to the successful suppression of charge recombination. It is worth mentioning that the *PCE* of the devices by using HPDT as the only ETL layer (15.84%) is a bit lower than that of PCBM, which could be attributed to the unsuitable thickness of HPDT resulting in the incomplete coverage on the surface of the perovskite layer.

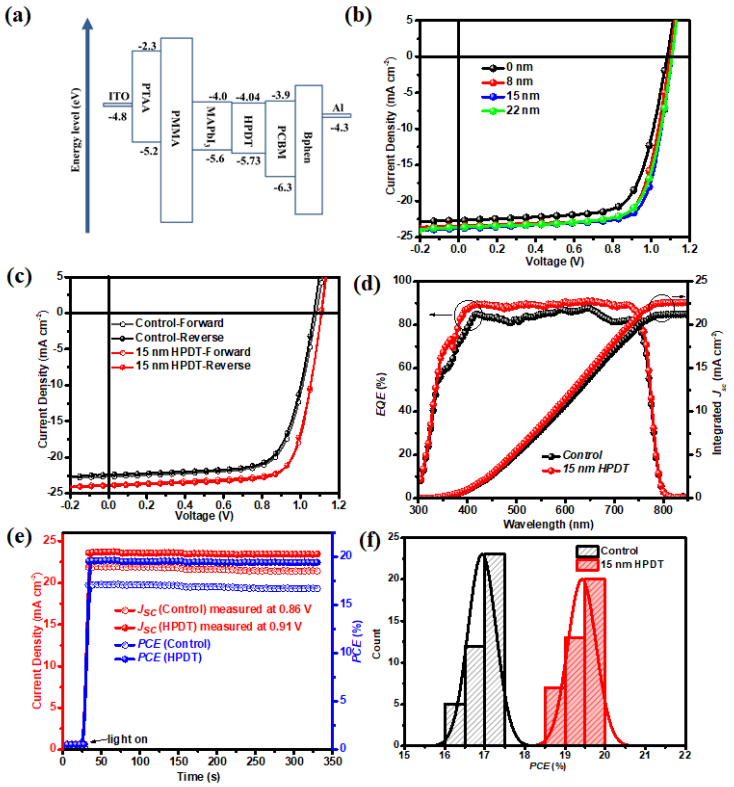

Figure 4. (a) Schematic structure of inverted PSCs; (b) champion *J-V* curves of PSCs with different thickness of the HPDT engineering layer; (c) *J-V* curves in forward and reverse scanning of the PSCs; (d) *EQE* curves and the integrated J_{sc} of PSCs; (e) stabilized photocurrent density and *PCE* output of the PSC with or without HPDT engineering layer; (f) *PCE* histograms of the PSCs with or without 15 nm HPDT interface engineering (40 independent devices for each condition).

The integrated J_{sc} was obtained by the external quantum efficiency (*EQE*) curves as shown in Figure 4d, indicating that the integrated J_{sc} values are in agreement with the *J-V*

measurement. The improvement of *EQE* spectra for HPDT engineered device could be attributed to the reduced trap density, decreased charge recombination, improved interface contact and improved electron mobility in the PSCs. Figure 4e shows the steady photocurrent and *PCE* measured at the maximum power output for the PSCs with or without HPDT. The steady photocurrent was 23.46 mA cm^{-2} and the stabilized *PCE* reached up to 19.45% for the PSCs with 15 nm HPDT, while the steady photocurrent was 21.43 mA cm^{-2} and the stabilized *PCE* reached up to 16.73% for the control PSCs, which agrees well with the *J-V* measurements. To provide an insight into the reproducibility and reliability of the devices, the *PCE* statistical distribution histograms of 40 devices are displayed in Figure 4f and Table S1. The average *PCE* values are 16.72±0.31% for control devices and 19.45±0.27% for the PSCs based on 15 nm HPDT, suggesting excellent reproducibility by HPDT interface engineering. In addition, we also fabricated the PSCs with the structure of ITO/PTAA:F4-TCNQ/PMMA /Perovskite/HPDT/PCBM/Al and ITO/PTAA:F4-TCNQ/PMMA/Perovskite/PCBM/Al. The *J-V* curve and detailed parameters are shown in Figure S13 and Table S2, respectively. The HPDT interface engineered devices without Bphen also shows enhanced performance along with a decreased hysteresis.

Table 2. Device performance of perovskite solar cells with or without 15 nm HPDT as interface engineering layer.

Condition	Scan direction	J_{sc} [mA cm^{-2}]	V_{oc} [V]	*FF* [%]	*PCE* [%]
HPDT	Forward	23.97	1.110	74.2	19.75
	Reverse	23.80	1.108	74.8	19.72
Control	Forward	22.67	1.084	70.7	17.38
	Reverse	22.37	1.070	71.2	17.03

3. Conclusion

In summary, a novel n-type small organic molecule, homologous perylene diimide tetramer (HPDT), was synthesized and used for interface engineering in the inverted perovskite solar cells. HPDT has higher electron mobility than PCBM that interface engineering enhanced the electron mobility of the ETL and decreased the recombination in PSCs. Furthermore, the performance of inverted $MAPbI_3$-based PSCs was greatly enhanced from 17.38% for control devices up to 19.75% for that with HPDT. This excellent performance is attributed to the suitable energy levels and high electron mobility of the HPDT layer, and reduced non-radiative recombination at the interface between perovskite layer and ETL. This work presents a novel method for interfacial engineering with conductive organic small molecules for high-performance PSCs.

Supporting Information

Supporting Information is available from the ELSEVIER.

Acknowledgements

This work has been partially supported by the National Key R&D Program of China (2018YFC0910602); the National Natural Science Foundation of China (61775145, 61525503, 61620106016, 61835009, 81727804); the China Postdoctoral Science Foundation Funded Project (2018M643147); (Key) Project of Department of Education of Guangdong Province (2015KGJHZ002, 2016KCXTD007); Guangdong Natural Science Foundation Innovation Team (2014A030312008); and Shenzhen Basic Research Project (JCYJ20170412110212234, JCYJ20160328144746940, JCYJ20170412105003520). W.-Y.W. would like to thank Science, Technology and Innovation Committee of Shenzhen Municipality (JCYJ20170303160036674); the Hong Kong Research Grants Council (PolyU

123384/16P, C5037-18G); Hong Kong Polytechnic University (1-ZE1C) and Ms. Clarea Au (847S) for the financial support.

Conflict of Interest

The authors declare no conflict of interest.

References

[1] T. Leijtens, G.E. Eperon, S. Pathak, A. Abate, M.M. Lee, H.J. Snaith, Overcoming ultraviolet light instability of sensitized TiO_2 with meso-superstructured organometal tri-halide perovskite solar cells, Nat. Commun. 4 (2013) 2885.

[2] H. Zhou, Q. Chen, G. Li, S. Luo, T.-b. Song, H.-S. Duan, Z. Hong, J. You, Y. Liu, Y. Yang, Interface engineering of highly efficient perovskite solar cells, Science 345 (2014) 542-546.

[3] K. Domanski, E.A. Alharbi, A. Hagfeldt, M. Grätzel, W. Tress, Systematic investigation of the impact of operation conditions on the degradation behaviour of perovskite solar cells, Nat. Energy 1 (2018) 61.

[4] A. Kojima, K. Teshima, Y. Shirai, T. Miyasaka, Organometal halide perovskites as visible-light sensitizers for photovoltaic cells, J. Am. Chem. Soc. 131 (2009) 6050-6051.

[5] NREL Efficiency chart, https://www.nrel.gov/pv/cell-efficiency.html.

[6] P. Wang, Y. Wu, B. Cai, Q. Ma, X. Zheng, W.-H. Zhang, Solution-processable perovskite solar cells toward commercialization: progress and challenges, Adv. Funct. Mater. 30 (2018) 1807661.

[7] A. Rajagopal, K. Yao, A.K.Y. Jen, Toward perovskite solar cell commercialization: a perspective and research roadmap based on interfacial engineering, Adv. Mater. 30 (2018) 1800455.

[8] M.M. Lee, J. Teuscher, T. Miyasaka, T.N. Murakami, H.J. Snaith, Efficient hybrid solar cells based on meso-superstructured organometal halide perovskites, Science 338 (2012) 643-647.

[9] X. Meng, J. Zhou, J. Hou, X. Tao, S. H. Cheung, S. K. So, S. Yang, Versatility of carbon enables all carbon based perovskite solar cells to achieve high efficiency and high stability, Adv. Mater. 30 (2018) 1706975.

[10] L. Huang, Z. Ge, Simple, robust, and going more efficient: recent advance on electron transport layer-free perovskite solar cells, Adv. Energy Mater. 9 (2019) 1900248.

[11] W. Hu, W. Zhou, X. Lei, P. Zhou, M. Zhang, T. Chen, H. Zeng, J. Zhu, S. Dai, S. Yang, S. Yang, Low-temperature in situ amino functionalization of TiO_2 nanoparticles sharpens electron management achieving over 21% efficient planar perovskite solar cells, Adv. Mater. 31 (2019) 1806095.

[12] F. Yang, D. Hirotani, G. Kapil, M.A. Kamarudin, C.H. Ng, Y. Zhang, Q. Shen, S. Hayase, All-inorganic $CsPb_{1-x}Ge_xI_2Br$ perovskite with enhanced phase stability and photovoltaic performance, Angew. Chem. Int. Ed. 57 (2018) 12745-12749.

[13] K.-H. Jung, J.-Y. Seo, S. Lee, H. Shin, N.-G. Park, Solution-processed SnO_2 thin film for a hysteresis-free planar perovskite solar cell with a power conversion efficiency of 19.2%, J. Mater. Chem. A 5 (2017) 24790-24803.

[14] J. Zhou, J. Wu, N. Li, X. Li, Y. Zheng, X. Tao, Efficient all-air processed mixed cation carbon based perovskite solar cells with ultra-high stability, J. Mater. Chem. A 7 (2019) 17594-17603.

[15] F. Wang, Y. Zhang, M. Yang, J. Du, L. Xue, L. Yang, L. Fan, Y. Sui, J. Yang, X. Zhang, Exploring low-temperature processed a-WO_x/SnO_2 hybrid electron transporting layer for perovskite solar cells with efficiency>20.5%, Nano Energy 63 (2019) 103825.

[16] Q. Dong, J. Li, Y. Shi, M. Chen, L. K. Ono, K. Zhou, C. Zhang, Y. Qi, Y. Zhou, N. P. Padture, L. Wang, Improved SnO_2 electron transport layers solution-deposited at near

room temperature for rigid or flexible perovskite solar cells with high efficiencies, Adv. Energy Mater. 9 (2019) 1900834.

[17] H. Guo, H. Chen, H. Zhang, X. Huang, J. Yang, B. Wang, Y. Li, L. Wang, X. Niu, Z. Wang, Low-temperature processed yttrium-doped $SrSnO_3$ perovskite electron transport layer for planar heterojunction perovskite solar cells with high efficiency, Nano Energy 59 (2019) 1-9.

[18] L. Yan, Q. Xue, M. Liu, Z. Zhu, J. Tian, Z. Li, Z. Chen, Z. Chen, H. Yan, H. L. Yip, Y. Cao, Interface engineering for all-inorganic $CsPbI_2Br$ perovskite solar cells with efficiency over 14%, Adv. Mater. 30 (2018) 1802509.

[19] Q. Jiang, X. Zhang, J. You, SnO_2: A wonderful electron transport layer for perovskite solar cells, Small 14 (2018) 1801154.

[20] K.A. Bush, A.F. Palmstrom, J.Y. Zhengshan, M. Boccard, R. Cheacharoen, J.P. Mailoa, D.P. McMeekin, R.L. Hoye, C.D. Bailie, T. Leijtens, 23.6%-efficient monolithic perovskite/silicon tandem solar cells with improved stability, Nat. Energy, 2 (2017) 17009.

[21] Y. Z. Zheng, E. F. Zhao, F. L. Meng, X. S. Lai, X. M. Dong, J. J. Wu, X. Tao, Iodine-doped ZnO nanopillar arrays for perovskite solar cells with high efficiency up to 18.24%, J. Mater. Chem. A 5 (2017) 12416-12425.

[22] J. Cao, B. Wu, R. Chen, Y. Wu, Y. Hui, B. W. Mao, N. Zheng, Efficient, hysteresis-free, and stable perovskite solar cells with ZnO as electron-transport layer: effect of surface passivation, Adv. Mater. 30 (2018) 1705596.

[23] P. Zhang, J. Wu, T. Zhang, Y. Wang, D. Liu, H. Chen, L. Ji, C. Liu, W. Ahmad, Z. D. Chen, S. Li, Perovskite solar cells with ZnO electron-transporting materials, Adv. Mater. 30 (2018) 1703737.

[24] J. Liu, C. Gao, L. Luo, Q. Ye, X. He, L. Ouyang, X. Guo, D. Zhuang, C. Liao, J. Mei, W. Lau, Low-temperature, solution processed metal sulfide as an electron transport layer for efficient planar perovskite solar cells, J. Mater. Chem. A 3 (2015) 11750-11755.

[25] W. A. Dunlap-Shohl, R. Younts, B. Gautam, K. Gundogdu, D. B. Mitzi, Effects of Cd diffusion and doping in high-performance perovskite solar cells using CdS as electron transport layer, J. Phys. Chem. C 120 (2016) 16437-16445.

[26] S. S. Shin, E. J. Yeom, W. S. Yang, S. Hur, M. G. Kim, J. Im, J. Seo, J. H. Noh, S. I. Seok, Colloidally prepared La-doped $BaSnO_3$ electrodes for efficient, photostable perovskite solar cells, Science 356 (2017) 167-171.

[27] X. Ye, H. Ling, R. Zhang, Z. Wen, S. Hu, T. Akasaka, J. Xia, X. Lu, Low-temperature solution-combustion-processed Zn-Doped Nb_2O_5 as an electron transport layer for efficient and stable perovskite solar cells, J. Power Sources (2019) 227419.

[28] Q. Jiang, X. Zhang, J. You, SnO_2: A wonderful electron transport layer for perovskite solar cells, Small 14 (2018) 1801154.

[29] L. Meng, J. You, T.-F. Guo, Y. Yang, Recent advances in the inverted planar structure of perovskite solar cells, Accounts Chem. Res. 49 (2015) 155-165.

[30] T. Liu, K. Chen, Q. Hu, R. Zhu, Q. Gong, Inverted perovskite solar cells: progresses and perspectives, Adv. Energy Mater. 6 (2016) 1600457.

[31] D. Luo, W. Yang, Z. Wang, A. Sadhanala, Q. Hu, R. Su, R. Shivanna, G.F. Trindade, J.F. Watts, Z. Xu, Enhanced photovoltage for inverted planar heterojunction perovskite solar cells, Science 360 (2018) 1442-1446.

[32] J. You, Z. Hong, Y. Yang, Q. Chen, M. Cai, T.-B. Song, C.-C. Chen, S. Lu, Y. Liu, H. Zhou, Low-temperature solution-processed perovskite solar cells with high efficiency and flexibility, ACS Nano 8 (2014) 1674-1680.

[33] C. Tao, S. Neutzner, L. Colella, S. Marras, A.R.S. Kandada, M. Gandini, M. De Bastiani, G. Pace, L. Manna, M. Caironi, 17.6% stabilized efficiency in low-temperature processed planar perovskite solar cells, Energy Environ. Sci. 8 (2015) 2365-2370.

[34] O. Malinkiewicz, A. Yella, Y.H. Lee, G.M. Espallargas, M. Graetzel, M.K. Nazeeruddin, H.J. Bolink, Perovskite solar cells employing organic charge-transport layers, Nature Photo. 8 (2014) 128.

[35] Y. Wu, X. Yang, W. Chen, Y. Yue, M. Cai, F. Xie, E. Bi, A. Islam, L. Han, Perovskite solar cells with 18.21% efficiency and area over 1 cm^2 fabricated by heterojunction engineering, Nat. Energy 1 (2016) 16148.

[36] X. Yin, P. Chen, M. Que, Y. Xing, W. Que, C. Niu, J. Shao, Highly efficient flexible perovskite solar cells using solution-derived NiO_x hole contacts, ACS Nano 10 (2016) 3630-3636.

[37] Y. Zheng, J. Kong, D. Huang, W. Shi, L. McMillon-Brown, H.E. Katz, J. Yu, A.D. Taylor, Spray coating of the PCBM electron transport layer significantly improves the efficiency of pin planar perovskite solar cells, Nanoscale 10 (2018) 11342-11348.

[38] J.J. van Franeker, K.H. Hendriks, B.J. Bruijnaers, M.W. Verhoeven, M.M. Wienk, R.A. Janssen, Monitoring thermal annealing of perovskite solar cells with in situ photoluminescence, Adv. Energy Mater. 7 (2017) 1601822.

[39] X. Liu, H. Yu, L. Yan, Q. Dong, Q. Wan, Y. Zhou, B. Song, Y. Li, Triple cathode buffer layers composed of PCBM, C_{60}, and LiF for high-performance planar perovskite solar cells, ACS Appl. Mater. Inter. 7 (2015) 6230-6237.

[40] Y. Bai, X. Meng, S. Yang, Interface engineering for highly efficient and stable planar p-i-n perovskite solar cells, Adv. Energy Mater. 8 (2018) 1701883.

[41] D. Liu, C.J. Traverse, P. Chen, M. Elinski, C. Yang, L. Wang, M. Young, R.R. Lunt, Aqueous-containing precursor solutions for efficient perovskite solar cells, Adv. Sci. 5 (2018) 1700484.

[42] S. Collavini, M. Saliba, W. R. Tress, P. J. Holzhey, S. F. Völker, K. Domanski, S. H. Turren-Cruz, A. Ummadisingu, S. M. Zakeeruddin, A. Hagfeldt, M. Grätzel, J. L. Delgado, Poly(ethylene glycol)-[60]fullerene-based materials for perovskite solar cells

with improved moisture resistance and reduced hysteresis, ChemSusChem 11 (2018) 1032-1039.

[43] J. Pascual, J. L. Delgado, R. Tena-Zaera, Physicochemical phenomena and application in solar cells of perovskite:fullerene films, J. Phys. Chem. Lett. 9 (2018) 2893-2902.

[44] J. Pascual, S. Collavini, S. F. Völker, N. Phung, E. Palacios-Lidon, L. Irusta, H. J. Grande, A. Abate, J. L. Delgado, R. Tena-Zaera, Unraveling fullerene-perovskite interactions introduces advanced blend films for performance-improved solar cells, Sustain. Energy Fuels 3 (2019) 2779-2787.

[45] D. Yang, X. Zhang, K. Wang, C. Wu, R. Yang, Y. Hou, Y. Jiang, S. Liu, S. Priya, Stable efficiency exceeding 20.6% for inverted perovskite solar cells through polymer-optimized PCBM electron-transport layers, Nano Lett. 19 (2019) 3313.

[46] Z. Zhu, Q. Xue, H. He, K. Jiang, Z. Hu, Y. Bai, T. Zhang, S. Xiao, K. Gundogdu, B.R. Gautam, A PCBM electron transport layer containing small amounts of dual polymer additives that enables enhanced perovskite solar cell performance, Adv. Sci. 3 (2016) 1500353.

[47] G. Kakavelakis, T. Maksudov, D. Konios, I. Paradisanos, G. Kioseoglou, E. Stratakis, E. Kymakis, Efficient and highly air stable planar inverted perovskite solar cells with reduced graphene oxide doped PCBM electron transporting layer, Adv. Energy Mater. 7 (2017) 1602120.

[48] Q. An, Q. Sun, A. Weu, D. Becker-Koch, F. Paulus, S. Arndt, F. Stuck, A.S.K. Hashmi, N. Tessler, Y. Vaynzof, Enhancing the open-circuit voltage of perovskite solar cells by up to 120 mV using π-extended phosphoniumfluorene electrolytes as hole blocking layers, Adv. Energy Mater. (2019) 1901257.

[49] M. Zhang, X. Zhan, Nonfullerene n-type organic semiconductors for perovskite solar cells, Adv. Energy Mater. (2019) 1900860.

[50] J. Zhang, Y. Li, J. Huang, H. Hu, G. Zhang, T. Ma, P.C. Chow, H. Ade, D. Pan, H. Yan, Ring-fusion of perylene diimide acceptor enabling efficient nonfullerene organic solar cells with a small voltage loss, J. Am. Chem. Soc. 139 (2017) 16092-16095.

[51] S. Fu, X. Li, L. Wan, Y. Wu, W. Zhang, Y. Wang, Q. Bao, J. Fang, Efficient passivation with lead pyridine-2-carboxylic for high-performance and stable perovskite solar cells, Adv. Energy Mater. (2019) 1901852.

[52] H. Zhang, Y. Wu, C. Shen, E. Li, C. Yan, W. Zhang, H. Tian, L. Han, W.H. Zhu, Efficient and stable chemical passivation on perovskite surface via bidentate anchoring, Adv. Energy Mater. 9 (2019) 1803573.

[53] H. Wang, L. Chen, Y. Xiao, Constructing a donor-acceptor linearconjugation structure for heterologous perylene diimides to greatly improve the photovoltaic performance, J. Mater. Chem. C 7 (2019) 835-842.

[54] H. Wang, L. Chen, Y. Xiao, Heterologous perylene diimide arrays: potential non-fullerene acceptors in organic solar cells, J. Mater. Chem. C 5 (2017) 8875-8882.